SAW Noise-Like Anti-Collision Code Study

N. Y. Kozlovski and D. C. Malocha
School of Electrical Engineering and Computer Science
University of Central Florida, Orlando, Florida 32816

***Abstract*— CDMA and OFC structures and coding schemes have typical correlation side lobes based on chip lengths, which makes it challenging to select good sets of codes for passive wireless SAW sensor systems. Presented in this paper is a new and novel SAW Noise-Like Reflector (NLR) with Pulse Position Modulation (PPM) for multi sensor systems with good auto- and cross-correlation, and anti-collision properties. NLR structures have no typical chips; it consists of a random sequence of varying width and pitch electrodes. Such structures are wideband and have very low correlation side lobes, which significantly reduces code collisions and simplifies code selection for a multi sensor system. A typical SAW NLR PPM sensor consists of a wideband transducer and a NLR PPM on one of the acoustic ports of the transducer. A second reflector bank can be added for differential sensor option. While these sensors can be extended to measure a variety of properties, a thermal sensor system was designed within the scope of this publication.**

This paper will discuss the basic analytic mathematical model used to predict the first order operation of NLR PPM sensors and the semi-random algorithm used to select code sequences with good anti-collision properties. A coupling of modes (COM) model was used to simulate sensors, and predict the performance of the sensor system more accurately. Both analytic mathematical and COM models yield close agreement, which verified that the simple model is a good synthesis tool and confirmed that the NLR PPM sensor design has the desired performance and advantage.

Experimental SAW NLR PPM sensors were built at 250MHz on YZ $LiNbO_3$. The system operates with an approximately 25% fractional bandwidth. Several sets of devices were fabricated with various codes and PPM parameters. Measured sensor data agreed well with both simple analytic mathematical and COM models. It is shown that this new NLR PPM structures a unique method for device coding and implementing SAW multi sensor spread spectrum systems.

I. Introduction

Extensive work has been done developing passive wireless SAW sensors using orthogonal frequency coding (OFC). A sample OFC device is shown in Fig. 1, the reflector bank consists of several OFC chips (3 shown as an example). Chip frequencies and time lengths are selected in such way that their frequency responses line up as shown in the frequency domain plot (Fig. 2). To allow for multiple sensors their frequencies (OFC chips) are shuffled for each device producing a unique code. A sample time domain response is shown in the Fig. 3 [1].

Work has been done on SAW sensor coding when large set of random code sets is generated with large number of codes, and then reduced to a smaller set with desired cross- and auto-correlation properties [2].

This paper will discuss coding technique that minimizes code collisions for systems with multiple sensors and also examine the possibility of using noise-like reflector (NLR) structures that could be used instead of OFC chips to improve the code collision and increase the number of codes.

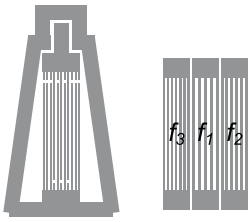

Fig. 1. Sample single-sided SAW sensor with 3 OFC chips.

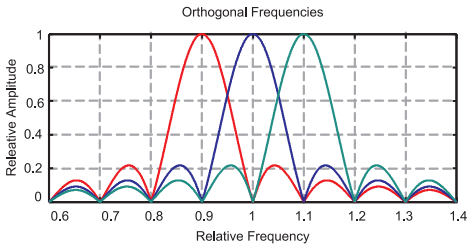

Fig. 2. Ideal example of a frequency domain response of a reflector of a sample single-sided SAW sensor with 3 OFC chips.

II. Modeling

A simple gated sine wave is used as the representation of a reflector bank or a single electrode (called a primitive structure) shown in equation (1),

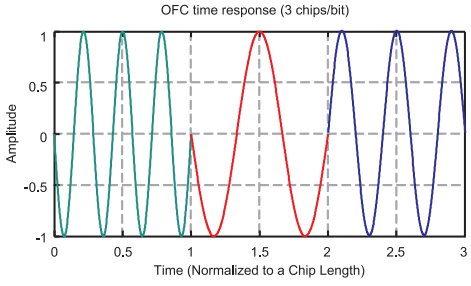

Fig. 3. Ideal example of a time domain response of a single-sided SAW reflector sensor with 3 OFC chips.

978-1-4244-3510-4/09/$25.00 ©2009 IEEE

$$h(t) = \sum_{k=1}^{N} Rect\left(\frac{t - \frac{\tau_{C_k}}{2} - \tau_{P_k}}{\tau_{C_k}}\right) \cdot Sin\left(2\pi f_k \left(\frac{t - \frac{\tau_{C_k}}{2} - \tau_{P_k}}{\tau_{C_k}}\right)\right) \quad (1)$$

where f_k is the frequency of the k^{th} primitive structure, τ_{P_k} is the position of the k^{th} primitive structure, τ_{C_k} length of the k^{th} primitive structure, and N is the number of primitive structures. This simple first order model has been previously demonstrated to be a good simulation and synthesis model [3].

A coupling of modes (COM) model was also used to simulate the devices. It has been basically shown that there is good correlation between first order model, COM model and experimental data for the structures designed and built for this publication [4], [3].

III. Temperature Extraction

A change of device temperature velocity translates into scaling of the frequency and the time domain responses. To measure the change in the surface velocity a set of matched filters is generated for different temperatures, which is basically the same function but scaled in time and frequency. Each of the matched filters is then correlated with the received response from the sensor. Matched filter with the highest correlation peak corresponds to the temperature of the sensor.

Shown in Fig. 4 is a brief overview of temperature extraction algorithm.

IV. Cell-based Device Coding

In a typical digital communication system a number of active components are designated to ensure that multiple devices do not conflict with each other. A base station typically tells the devices when to talk, when not to talk, how much power to output and which frequency to use. This is done through the handshaking and the ongoing monitoring of the devices within the environment. Also, when the received digital signal is correlated, shape and quality of the correlation peak is not as important as long as it is detectable and the phase can be determined.

In a passive wireless system once the device is in place it will use fixed frequencies at fixed times and output (reflected) power that cannot be controlled by the base station. Correlation of the sensor of interest is computed together with cross-correlations of all the other devices present in the system. In order to extract temperature accurately, the auto-correlation peak must be unaffected by the presence of all the other cross-correlations. In other words, cross-correlations of other devices needs to be minimal (ideally zero) in the proximity of the main auto-correlation peak.

Codes must be designed in such way that at any given time each sensor is either silent or occupies its own frequency band(s). An OFC device is composed of a number of OFC chips and the location of the chips are assigned time slots. For multiple OFC devices operating without collisions, for any one given time slot are OFC chip of a certain frequency can only be used in one device.

A relationship can be established between the number of chips used to make up one device (n), number chip that are allowed to be used within the same time slot (m), number of devices required (N), and number of time slots (M) as shown in equation (2).

$$M = \left\lceil N \cdot \frac{n}{m} \right\rceil \quad (2)$$

Fig. 5 shows 16 codes for a 16-device system, that uses seven OFC chips. In the table each row is a code, each column is a OFC-chip length time slot. Cells with zeros are unused time slots of a particular code and cells with values 1-7 are time slots with OFC chips of orthogonal frequencies 1-7.

Fig. 6 shows the schematic drawing of how the first two codes of Fig. 5 would be implemented into actual devices. The 16-code system was then simulated using the first order model discussed in section II. In Fig. 7 an auto-correlation of one device (blue) was compared to the correlation of the matched filter for that device to the entire system with all the 16 codes (green). It can be noted that the main auto-correlation peak was not affected significantly by the presence of all the cross-correlations. Also note that even the two main side-lobes of

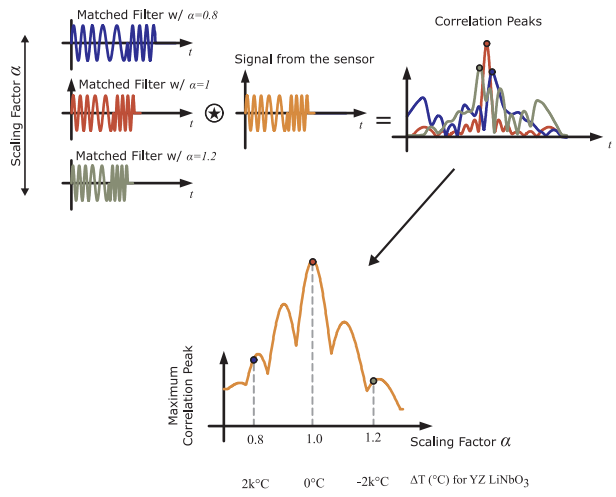

Fig. 4. Temperature extraction principle.

Time Slot Number (M=16)

Device Number (N=16)	1	2	3	4	5	6	7	8	9	10	11	12	13	14	15	16
1	0	0	7	5	3	0	0	0	6	0	0	2	0	1	0	4
2	4	5	0	0	0	2	6	7	0	1	3	0	0	0	0	0
3	5	4	3	6	0	0	0	0	0	0	7	0	1	0	2	0
4	0	0	0	0	5	0	1	3	0	2	0	0	6	4	0	7
5	0	0	0	0	0	3	0	5	2	7	0	1	0	6	4	0
6	7	0	4	3	1	6	2	0	0	0	0	0	0	0	5	0
7	0	6	0	0	0	7	0	0	1	0	5	3	4	0	0	2
8	2	7	1	0	6	0	3	0	0	0	0	4	0	5	0	0
9	0	0	0	0	0	0	0	4	3	5	6	0	2	0	7	1
10	0	0	0	1	2	5	7	0	0	4	0	6	0	0	3	0
11	0	3	6	2	0	0	0	1	0	0	4	0	5	7	0	0
12	1	0	0	0	7	0	5	0	4	0	0	0	0	2	6	3
13	0	0	2	4	0	1	0	0	5	0	0	7	3	0	0	6
14	6	1	5	7	0	0	4	0	0	3	2	0	0	0	0	0
15	3	0	0	0	4	0	0	2	0	6	0	0	7	0	1	5
16	0	2	0	0	0	4	0	6	7	0	1	5	0	3	0	0

Fig. 5. A sample set of 16 OFC devices using 16 time slots and 7 frequencies.

the auto-correlation have not been affected significantly, which means that even if the location of the auto-correlation peak shifts due to a temperature change, within a certain distance it still will not collide with the other cross-correlations. The amount by which the peak can change its position while been unaffected is one of the factors that will determine the dynamic range of the system and its physical spread in space. Even though only one device is demonstrated, this is representative of all the 16 devices. This cell-based approach to device coding produces codes with excellent anti-collision properties.

V. NLR Structures and Device Scaling

Previous work has shown that the noise-like reflector (NLR) structures are wide-band with random pass- and reflect-bands and can produce codes with good auto-correlation and anti-collision properties [3]. At this time such reflectors are generated randomly. Once a set of devices with NLR structures is generated each cross-correlation needs to be examined for the anti-collision properties. If one or more of the cross-correlations do not have the desired anti-collision properties, the entire set has to be discarded and a new one is generated until all cross-correlations are satisfactory. For sets with large number devices and large number of electrodes this code set selection process could be time and resource consuming.

Proposed in this section is a new and novel approach for the code generation where instead of the OFC chips NLR chips are used. The chips are much shorter than the entire code and fewer chips are needed to build up larger number of codes, which significantly reduces time and resources needed for good NLR chip selection.

First, it is important to establish how a NLR chip is constructed. Shown in Fig. 8 is a diagram of a portion of a NLR chip. The NLR structure is created by taking a regular reflector bank and inserting free space (shown in blue) between electrode-gap pairs (shown in red and light red). As the amount of inserted free space increases, anti-collision properties improve. In this particular case quarter-wavelength electrodes are used, making an electrode-gap pair half-wavelength long. Inserted free space is an integer multiple (shown as K in Fig. 8) of a quarter-wavelength, which makes electrodes randomly in-phase or 180° out of phase.

Two OFC chips with adjacent frequencies have cross-correlation lobes to main auto-correlation peak ratio of 0.3. Same ratio for two OFC chips with one over adjacent frequencies is 0.2. Since NLR chips are random, only probability of having cross-correlation lobes to main auto-correlation peak ratio below a certain level can be determined: analytical expression is difficult to calculate; it would have to factor in the electrodes representation as sine waves and the band-limiting transducer effect. It is, however, possible to determine this probability by analyzing large numbers of NLR chips sets. Fig. 9 shows the probability for two NLR chips; each chip has 16 electrodes at 250MHz center frequency randomly distributed within 312ns window with average integer multiple for inserted free space K=7.75 and a 150MHz null-bandwidth transducer.

From Fig. 9 it can be noted that it is possible to find two chips with cross-correlation lobes lower than 20%, which is comparable to OFC chips. In order to compete with the OFC approach it is needed to find more NLR chips. For N NLR chips the number of cross-correlations needed to be examined is $\frac{1}{2}\left(N^2 - N\right)$. After generating and analyzing numerous 4-NLR-chip sets a few sets were found where maximum cross-correlation lobes were below 30% of the average of the four auto-correlation peaks of their respective NLR chip set.

The odds of finding good codes rapidly decreases with the number of codes needed. One way to produce more codes is to simply scale the physical dimensions of the reflector bank leaving the code the same. Fig. 10 shows the maximum cross-correlation lobe when correlating one code with its scaled versions. If a code is scaled to 1.01 (by 1%) of its original physical dimensions, maximum cross-correlation is reduced to 10% of the auto-correlation peak. Scaling physical dimensions of a 250MHz device by factor of 1.04 produces a 260MHz

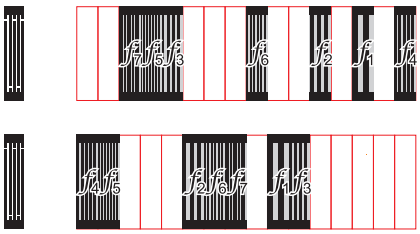

Fig. 6. Two sample devices realized using codes 1 and 2 from Fig. (5).

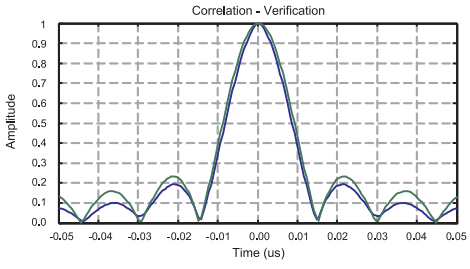

Fig. 7. Comparison of auto-correlation of a single device to correlation of that device to the entire system (sum of 16 devices.)

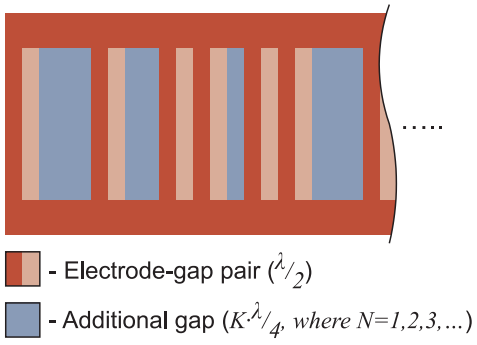

Fig. 8. Construction of a NLR chip

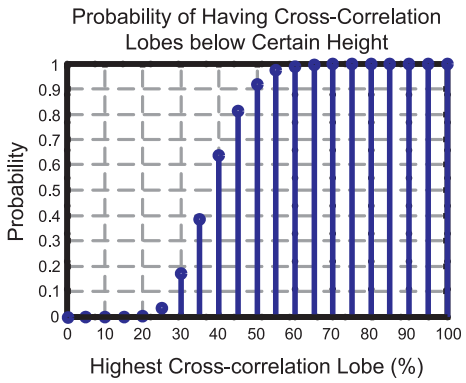

Fig. 9. Probability of having highest cross-correlation lobe of a certain percent of auto-correlation peak.

device, similar to OFC chips.

Note that this process of forming the chips is similar to the temperature extraction algorithm described in section III. It is possible to change the temperature of one sensor such that one of its chips will work at a frequency of another chip of another sensor in the system that is designed to work at a different frequency. This is also true of the OFC-based devices. The desired dynamic range of the system needs to be taken under consideration when using chip scaling approach for device design.

A 12-sensor system was designed using the NLR approach with scaling and simulated using the first order model discussed in section II. Four unique NLR chips were randomly generated and selected based on having all cross-correlation lobes to main auto-correlation peak rations below 0.3. Each NLR chip consists of 16 electrodes at 250MHz center frequency randomly distributed within a 312ns window with an average integer multiple for inserted free space K=7.75. These codes where scaled to two more frequencies (240MHz and 260MHz), producing a total of 12 NLR-chips. An unapodized transducer with 150MHz null-bandwidth used in simulation

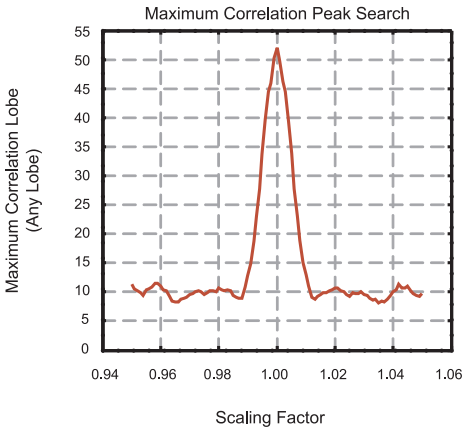

Fig. 10. Highest correlation lobe of correlation of one NLR chip to the another NLR chip with the same code but scaled to a different frequency.

and with four NLR chips per device were used. The number of time slots needed was determined to be 4 based on equation (2). The codes are shown in Fig. 11, where each row is a code and each column is a time slot. In this case each NLR-chip (cell) is denoted by two numbers (f, g), where f is the NLR code number 1 through 4 and g is an index of the frequency used: 1, 2 and 3 that correspond to 240MHz, 250MHz and 260MHz, respectively.

Shown in Fig. 12 is the auto-correlation of one of the 12 codes compared to the correlation of that code to the entire system (sum of all the 12 codes). Shown is an average performing device in terms of the anti-collision properties. The main correlation peak of the code to the system shown in Fig. 12 is approximately 4% lower than the auto-correlation of just that one code by itself, which is indicative of code collision, also the presence of the cross-correlation lobes close to the auto-correlation peak indicates potentially smaller dynamic range of the NLR-based system than in the case of the OFC-based system.

VI. Experimental Work

A. OFC-based System

In order to assess the differences in the performance of the NLR-based and the OFC-based approaches the two code sets were designed to have as many parameters in common as possible. The OFC-based system was designed after the NLR-based system described in section V. The following parameters were used for both systems and as similar as possible: number of the electrodes per reflector bank, time length of each reflector bank, and a wide-band transducer. One of the possible solutions for the OFC-based system meeting these requirements consisted of three OFC chips (240MHz, 250MHz and 260MHz with 25, 26 and 27 electrodes respectively), each chip had time response length of 0.104μs. In order to produce 12 codes, 12 time slots and 3 chips per device were used. Each device has 78 electrodes and on average approximately 1.04μs time response length. Codes used for the OFC-based system are shown in Fig. 13. Three of the 12 devices were fabricated on YZ $LiNbO_3$.

Since the temperature is most likely to vary versus the time the measurement is performed, temperature extraction was

Time Slot Number (M=4)

Device Number (N=12)	1	2	3	4
1	(4,2)	(2,2)	(4,3)	(2,1)
2	(1,2)	(1,3)	(2,3)	(3,1)
3	(1,3)	(3,3)	(4,1)	(1,1)
4	(4,3)	(2,3)	(1,3)	(3,3)
5	(2,2)	(2,1)	(1,1)	(1,2)
6	(4,1)	(4,2)	(2,2)	(3,2)
7	(3,2)	(3,1)	(3,3)	(4,3)
8	(3,3)	(4,3)	(2,1)	(2,3)
9	(1,1)	(3,2)	(1,2)	(4,1)
10	(2,1)	(1,2)	(3,2)	(1,3)
11	(3,1)	(1,1)	(4,2)	(2,2)
12	(2,3)	(4,1)	(3,1)	(4,2)

Fig. 11. NLR-based code set, each NLR chip is denoted by two numbers (f, g), where f is NLR code number and g is an index of the frequency used.

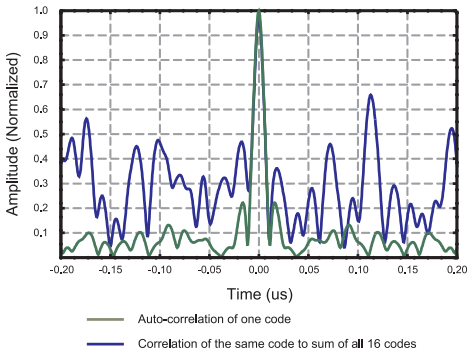

Fig. 12. Comparison of auto-correlation of a single device to correlation of that device to the entire system (sum of 12 devices.)

Time Slot Number (M=12)

Device Number (N=12)	1	2	3	4	5	6	7	8	9	10	11	12
1	0	1	0	0	3	2	0	0	0	0	0	0
2	1	0	0	0	0	0	0	0	0	0	3	2
3	0	0	0	1	0	0	2	0	3	0	0	0
4	0	0	0	2	0	0	0	3	1	0	0	0
5	2	0	0	0	0	1	0	0	0	3	0	0
6	0	3	2	0	0	0	1	0	0	0	0	0
7	0	0	0	0	2	3	0	0	0	0	1	0
8	0	0	1	3	0	0	0	2	0	0	0	0
9	3	0	0	0	0	0	0	0	2	1	0	0
10	0	0	0	0	0	0	3	0	0	0	2	1
11	0	0	0	0	1	0	0	0	0	2	0	3
12	0	2	3	0	0	0	0	1	0	0	0	0

Fig. 13. OFC-based code set, each cell with number 1, 2 or 3 corresponds to an OFC chip with center frequency 240MHz, 250MHz or 260MHz respectively, and each cell with zero corresponds to an unused time slt for that particular device

performed as described in section III. Fig. 14 compares the correlation of the measured and the ideal responses and the auto-correlation of the ideal response. The plot shows very good agreement between the first order model and the experimental data. The two other devices were also measured and added to the first measured device. This sum was correlated against the ideal response of the first device and compared the ideal auto-correlation of that device as shown in Fig. 15. It can be noted that while the two adjacent lobes to the main peak did go up, the peak is not affected by the presence of the two other devices. This very well demonstrates the anti-collision properties of the OFC-based devices coded using the cell-based approach.

B. NLR-based System

The NLR-based system was built using codes described in section V. The electrode count per reflector bank is 64 and average time length response is approximately 1.2μs. Three of the 12 devices were built on YZ $LiNbO_3$.

Fig. 16 compares the correlation of the measured with the ideal response, and the auto-correlation of the ideal response. Plot shows good agreement between the first order model and the experimental data. The two other devices were then measured and added to the first measured device. This sum was correlated against the ideal response of the first device and compared the ideal auto-correlation of that device as shown in Fig. 17. It can be noted that the peak was not affected by the

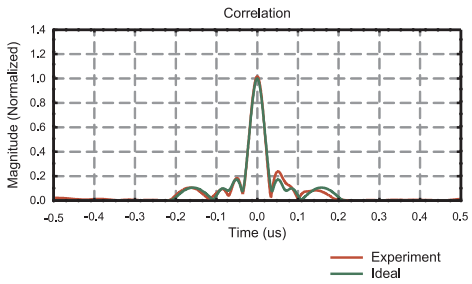

Fig. 14. Comparison of auto-correlation of an ideal OFC device (green) to correlation of ideal device response and experimental data for that device (red).

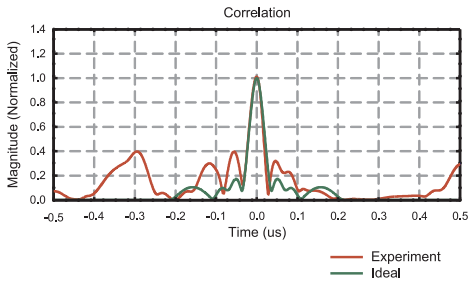

Fig. 15. Comparison of auto-correlation of a single ideal OFC device response to correlation of ideal OFC device response and sum of 3 devices measured experimentally.

presence of the two other devices; however, a cross-correlation lobe appeared at the base of the auto-correlation peak. At fixed temperature it is demonstrated that the NLR-based approach provides good anti-collision codes. It can also be noted that the auto-correlation peak of the NLR device is narrower than the auto-correlation peak of the OFC device, which translates into higher sensitivity to a temperature change.

VII. Conclusion

Cell-based coding produces codes with excellent anti-collision properties. In case of the OFC chips, cross-correlation lobes in the proximity of the main auto-correlation lobe are generally very low resulting in a good dynamic range of the system. NLR chips along with chip scaling can produce even larger amount of codes in the system. The drawback

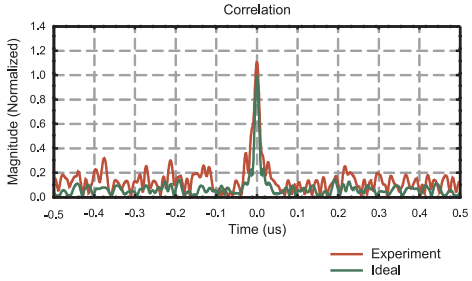

Fig. 16. Comparison of an ideal NLR device (green) to correlation with the ideal device response, and experimental data for that device (red).

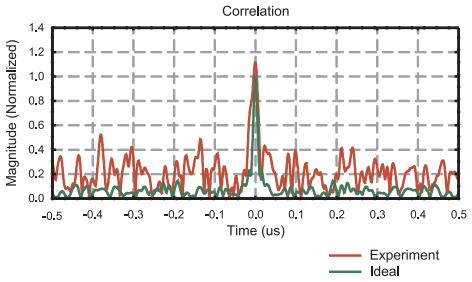

Fig. 17. Comparison of auto-correlation of a single ideal NLR device response to correlation of ideal NLR device response and sum of 3 devices measured experimentally.

of the NLR-based approach is reduced dynamic range. Auto-correlation peak of NLR devices is narrower compared to OFC devices, which yields higher sensitivity. It is possible to use this approach on the substrate that is less sensitive to the temperature change. Decreased sensitivity of the substrate can reduce the collision problem of the NLR codes and can be compensated by the increased sensitivity of these devices. The NLR-based approach has better security properties and on temperature compensated substrate can work well as a RFID tag.

Good agreement has been shown between the first order model and the experimental data. The first order model provides a good synthesis and simulation tool.

ACKNOWLEDGMENT

This work has been supported by NASA's Florida Space Grant Consortium Fellowship.

REFERENCES

[1] D. Malocha, D. Puccio, and D. Gallagher, "Orthogonal frequency coding for SAW device applications," in *Ultrasonics Symposium, 2004 IEEE*, vol. 2, 23-27 Aug. 2004, pp. 1082–1085Vol.2.

[2] E. Dudzik, A. Abedi, D. Hummels, and M. da Cunha, "Orthogonal code design for passive wireless sensors," in *Proc. 24th Biennial Symposium on Communications*, 2008, pp. 316–319.

[3] N. Kozlovski and D. Malocha, "Saw noise-like coded reflector structures," in *Proc. IEEE International Frequency Control Symposium*, 2008, pp. 290–295.

[4] B. P. Abbott, "A coupling-of-modes model for SAW transducers with arbitrary reflectivity weighting," Ph.D. dissertation, University of Central Florida, 1989.